Volume 74 (2018)

Supporting information for article:

X-ray reflectivity of chemically vapor-deposited diamond single crystals in the Laue geometry

S. Stoupin, J. P. C. Ruff, T. Krawczyk and K. D. Finkelstein

Supporting information

I. VALIDATION OF THE EXPERIMENTAL SETUP

A. Parameters of the double-crystal non-dispersive experimental configuration

TABLE I: Parameters of reflections involved in the measurements of absolute reflectivity of CVD diamond plates at 15keV:
η - asymmetry angle of the reflection,
b_H - asymmetry ratio of the reflection,
θ_c - angle of the center region of the reflection (approximately equal to the Bragg angle),
$\Delta\theta$ - angular width of the reflection region at entrance,
$\Delta\theta'$ - angular width of the reflection region at exit.
The angular widths are given in zero absorption approximation for perfect crystals and σ-polarization of the X-ray wave.

Reflection	Si 220	C $\bar{1}\bar{1}\bar{1}$	C $\bar{1}\bar{1}1$
η [deg]	10.5	54.7	54.7
b_H	-0.086	0.75	1.34
θ_c [deg]	12.4	11.6	11.6
$\Delta\theta$ [μrad]	42	13.5	10.1
$\Delta\theta'$ [μrad]	3.7	10.1	13.5

B. Reflectivity of HPHT diamond plates in the Laue geometry at 15 keV

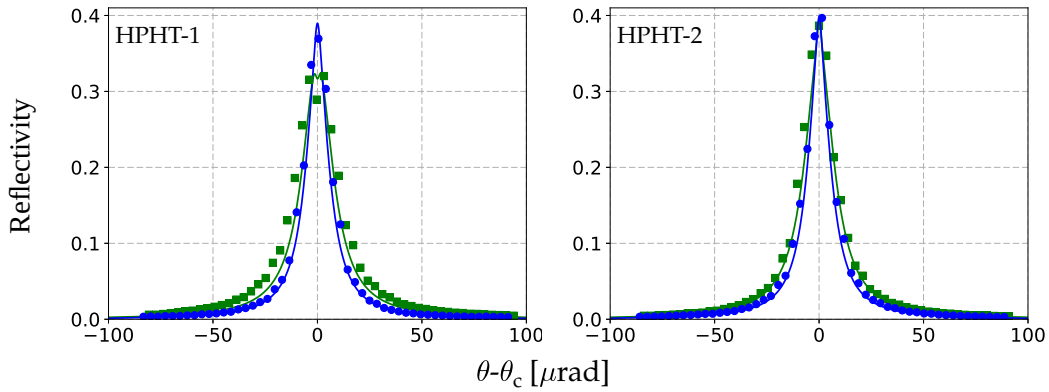

FIG. 1: Reflectivities of HPHT diamond plates measured in the Laue geometry (Fig. 4 of the article). Data measured in the beam expanding geometry is shown with squares(green) while data measured in the beam compressing geometry is shown with circles (blue). The green and blue solid lines represent theoretical reflectivity curves (dynamical theory of X-ray diffraction for perfect crystals) of beam expanding and beam compressing geometry respectively. Matching the theoretical curves to the experimental data was achieved by convolution of the theoretical curves with Lorentzian function, which approximated angular spread of radiation at the exit of the Si 220 asymmetric crystal (beam conditioner) and minor variation of the thicknesses of crystal plates (few microns) from their nominal values (550 μm).

Reflectivities of two similar HPHT crystals (crystals described in Table 2 of the article) were measured in the same experimental arrangement using incident beam with the same size of 1×1 mm^2. The probed regions were approximately centered on the entrance surface of the crystals. The measured reflectivities for the 111 reflection are shown in Fig.1 for beam expanding geometry (green squares) and for beam compressing geometry (blue circles). Theoretical curves were calculated using dynamical theory of X-ray diffraction for perfect crystals and convoluted with a Lorentzian function of 4 μrad width, which approximates the instrument resolution function defined by the exit angular width of the Si 220 asymmetric beam conditioner. It was found that the shape of the convoluted curve

strongly depends on the thickness of the diamond plate. Thickness variations of a few microns from the nominal value yield satisfactory agreement between theory and experiment. The discrepancies in the shape of the curve can be attributed to imperfections of the beam conditioner crystal (surface preparation), drift of the angular scale (goniometer imperfections) and imperfections in the studied HPHT plates.

Rocking curve topographs of the studied crystal regions are shown in Fig. 2 for plate HPHT-1 and in Fig. 3 for plate HPHT-2. The subplots (a) and (b) in these figures correspond to beam expanding and beam compressing geometries respectively. The crystals are nearly strain-free as evidenced by $\delta\theta_m$ topographs (average deviations of $\approx 1\mu$rad and only a few localized strong deviations). Crystal defects at low concentrations (compared to any of the CVD plates) are present in both HPHT plates. Correlating the discrepancies in the shapes of the reflectivity curves to the rocking curve topographs at these levels is speculative. A general remark that presence of crystal defects increases the width of the reflectivity curves above the theoretical values still applies. Systematic gradients in the peak position of the local rocking curves were not observed over the studied crystal volume. Thus, effects of long-range lattice bending on the width of the reflectivity curve can be excluded. Overall, the theory and experiment are in reasonable agreement for the HPHT crystals. The uncertainties in the measured angular characteristics (best described as long-term drifts of the angular scale of the goniometer) were on the order of a few microradians per hour, which is acceptable for characterization of CVD diamond plates with much larger values of local lattice misorientations.

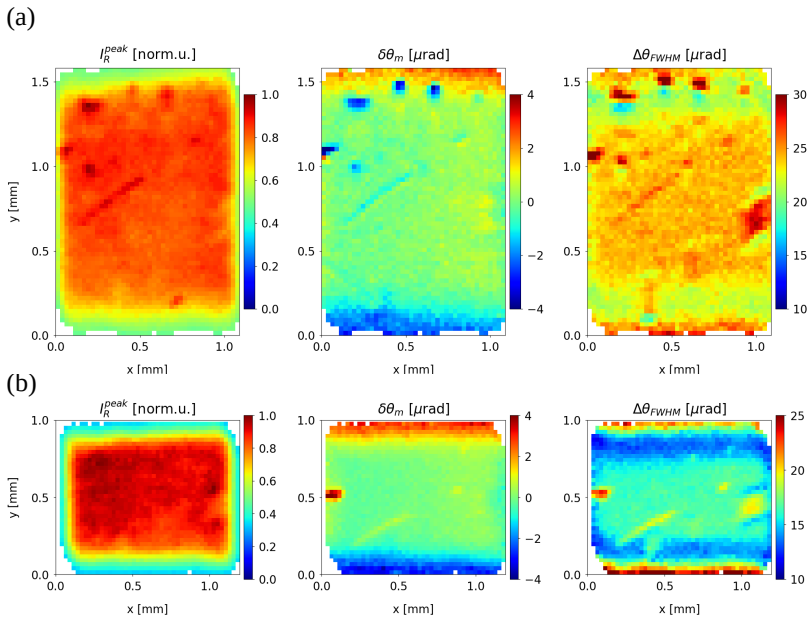

FIG. 2: Rocking curve topographs of plate HPHT-1 in the selected region probed with the 1×1 mm^2 beam in the beam expanding geometry (a) and in the beam compressing geometry (b) representing maps of the reflected intensity as the curve's peak value normalized by the maximum value observed (I_R^{peak}), the curve's peak position ($\delta\theta_m$) and the curve's width as a full width at half maximum ($\Delta\theta_{FWHM}$).

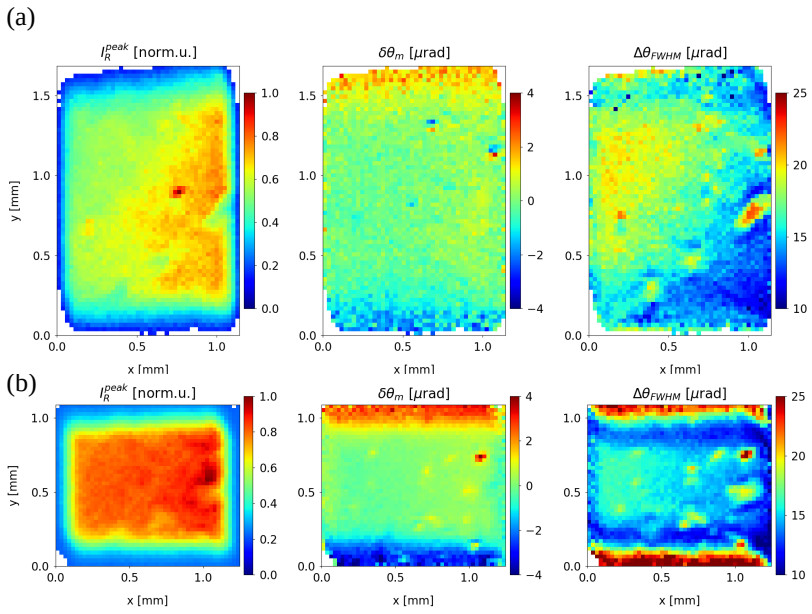

FIG. 3: Rocking curve topographs of plate HPHT-2 in the selected region probed with the 1×1 mm^2 beam in the beam expanding geometry (a) and in the beam compressing geometry (b) representing maps of the reflected intensity as the curve's peak value normalized by the maximum value observed (I_R^{peak}), the curve's peak position ($\delta\theta_m$) and the curve's width as a full width at half maximum ($\Delta\theta_{FWHM}$).

II. REFLECTIVITY CURVES OF PLATE CVD-4 AT 15 KEV

Figure 4 shows reflectivities of plate CVD-4 measured in the same experimental arrangement at 15 keV. Data measured in the beam expanding geometry is shown with squares(green) while data measured in the beam compressing geometry is shown with circles (blue). The curves exhibit broadening of a few microradians but otherwise are similar to those of HPHT diamond plates. The green and glue solid lines represent matching solutions of Darwin-Hamilton equations with adjusted Δ_0 and t_0 parameters shown in Table 3 of the article. As discussed in the article the use of Darwin-Hamilton equations is not justified due to the large required values of t_0 comparable with the thickness of the diamond plate. The density of defects is not sufficient to describe the crystal microstructure using continuous functions. These values of t_0 could still be interpreted as characteristic distances of coherent interaction of the X-ray wavefields with the crystal lattice.

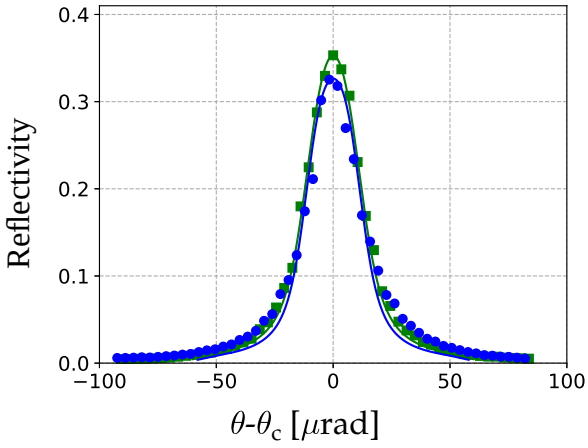

FIG. 4: Reflectivities of CVD-4 diamond plate measured in the Laue geometry (Fig. 4 of the article). Data measured in the beam expanding geometry is shown with squares(green) while data measured in the beam compressing geometry is shown with circles (blue). The green and blue solid lines represent theoretical reflectivity curves (solutions of the Darwin-Hamilton equations) of beam expanding and beam compressing geometry respectively. Matching the theoretical curves to the experimental data was achieved by adjustment of the mosaic block thickness t_0 and the standard deviation of angular misorientation Δ_0.

III. REFLECTIVITY CURVES OF PLATE CVD-3 AT 8 KEV

Verification of the theoretical model was performed using rocking curve topography data collected for a subset of studied plates at a different photon energy. Data collection was performed in the Laue geometry at a photon energy of 8 keV using rocking curve topography setup at beamline 1-BM of the Advanced Photon Source [1]. Two different beam conditioner crystals were used: Si 220 with asymmetry angle 22 deg for measurements of diamond 111 reflectivity and Si 331 with asymmetry angle 36.2 deg for measurements of diamond 220 reflectivity. The measurement in the Si 331 - C 220 configuration was performed at slightly different photon energy of 8.2 keV to increase the asymmetry ratio, which further reduced the size of the reflection region at the exit of the beam conditioner and provided more uniform illumination of the diamond plate. In these experiments intensities of the incident and reflected beams were not measured simultaneously using calibrated detectors. The measured reflectivities were extracted from rocking curve topographs as reflected intensity averaged over the region corresponding to 1×1 mm^2 incident beam centered on the crystal (reasonably matching the crystal regions illuminated in the experiment at 15keV). The incident intensity monitor (an ionization chamber monitoring X-ray flux after the beam conditioner) was available which permitted normalization and therefore relative comparison of the reflectivity curves. While a single scaling factor was possible for the two cases of the 111 reflection, reflectivities of measured in the Si 331 - C 220 configuration required an independent scaling factor (due to different asymmetry ratio of the beam conditioner).

Figure 5(111) shows $\bar{1}\bar{1}\bar{1}$ reflectivity in the beam expanding geometry (green squares) and $\bar{1}\bar{1}1$ reflectivity in the beam compressing geometry (blue circles). The green and blue solid lines represent theoretical calculations at 8 keV in beam compressing and beam expanding geometries respectively using Δ_0 and t_0 parameters obtained in matching theory and experiment at 15 keV (Table 3 of the article). The theory and the experiment are in a reasonable agreement. A slight discrepancy in the maximum reflectivity values could be attributed to absorption in the polyimide sample holder which was taken into account using tabulated data [2] of the nominal holder thickness rather than direct measurement. Figure 5(220) shows 220 reflectivities evaluated using two different regions of the crystal: a 1×1 mm^2 region centered on the crystal as shown by the dashed box in rocking curve topographs (Fig. 6) and a similar region shifted by 0.6 mm towards the bottom of the crystal, where elevated levels in the peak position $\delta\theta_m$ and curve width $\Delta\theta_\sigma$ are observed (dotted box in Fig. 6). The green solid curve represent theoretical calculation at 8.2 keV using Δ_0 and t_0 parameters obtained at 15 keV in the beam expanding geometry while the blue curve represents theoretical calculation using these parameters obtained in the beam compressing geometry. As discussed in the article, the discrepancies between the two sets are due to different illuminated crystal volumes, where the lower portion of the crystal is illuminated in the beam compressing geometry. The reasonable agreement between theory and experiment obtained for the 220 reflection at a different photon energy confirms this conclusion.

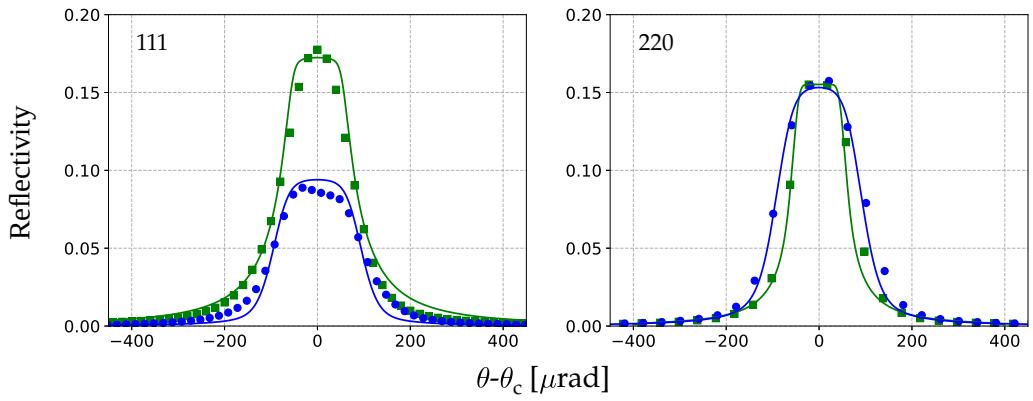

FIG. 5: Reflectivitiy of CVD-3 diamond plate measured in the Laue geometry at 8 keV: (111) reflectivity evaluated from experimental data in the beam expanding geometry is shown with squares(green) and reflectivity evaluated from experimental data in the beam compressing geometry is shown with circles (blue). The green and blue solid lines represent theoretical reflectivity curves of the beam expanding and the beam compressing geometry respectively calculated using corresponding Δ_0 and t_0 parameters obtained in matching theory and experiment at 15 keV (Table II of the article); (220) reflectivity corresponding to the crystal region marked by the dashed box (green squares) in Fig.6 and reflectivity corresponding to a similar region shifted towards the lower portion of the crystal by 0.6 mm (blue circles). This region is marked by the dotted box in Fig. 6. The green solid curve represent theoretical calculation at 8.2 keV using Δ_0 and t_0 parameters obtained at 15 keV in the beam expanding geometry while the blue curve represents theoretical calculation using these parameters obtained in the beam compressing geometry.

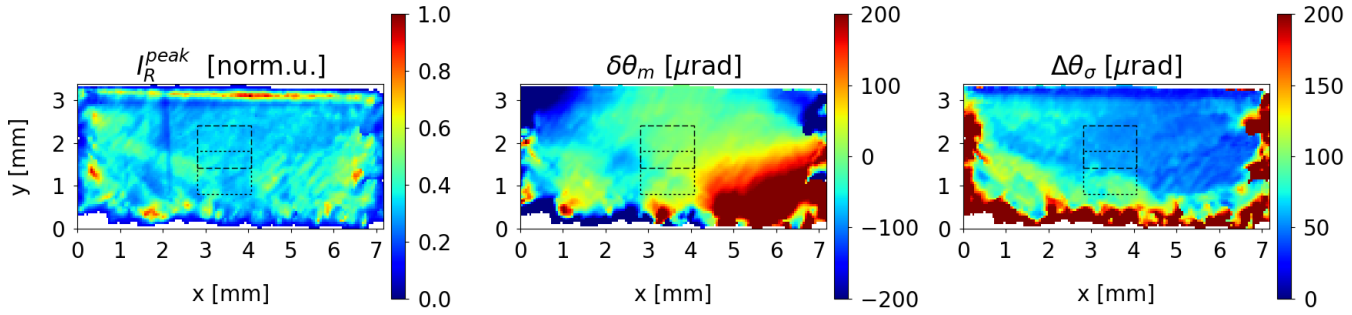

FIG. 6: Rocking curve topographs of plate CVD-3 corresponding to 220 Laue symmetric reflection at 8.2 keV: map of the reflected intensity as the curve's peak value normalized by the maximum value observed (I_R^{peak}), the curve's peak position ($\delta\theta_m$) and the curve's width as a standard deviation of a Gaussian approximation ($\Delta\theta_\sigma$). Scaled averaged reflected intensities from the two 1×1 mm^2 regions marked by the dashed and dotted boxes are shown in Fig.5 by green squares and blue circles respectively.

[1] S. Stoupin, Yu. Shvyd'ko, E. Trakhtenberg, Z. Liu, K. Lang, X. Huang, M. Weiczorek, E. Kasman, J. Hammonds, A. Macrander, et al., AIP Conf. Proc. **1741**, 050020 (2016).
[2] B. Henke, E. Gullikson, and J. Davis, Atomic Data and Nuclear Data Tables **54**, 181 (1993), http://henke.lbl.gov/optical_constants/.